MRS Advances (2025) 10:1813–1818
https://doi.org/10.1557/s43580-025-01209-8

ORIGINAL PAPER

A synchrotron X-ray diffraction and electron microscopy study of vanadium-doped UO_2

Gabriel L. Murphy[1] · Julien Marquardt[2] · Martina Klinkenberg[1] · Daniil Shirokiy[1] · Philip Kegler[1] · Maximilian Henkes[1] · Andrey Bukaemskiy[1] · Selina Richter[3] · Luiza Braga[3] · Christoph Hennig[3,4] · Dirk Bosbach[1]

Received: 23 January 2025 / Accepted: 13 February 2025 / Published online: 24 February 2025

Abstract

The doping of UO_2 ceramics with transition metal elements such as vanadium is a topical enterprise due to the relevance to advanced technology nuclear fuels in addition to understanding fuel-cladding interactions in spent nuclear fuel. Herein, the lattice and microstructural dependence of V-doped UO_2 ceramics synthesized under conditions of − 420 kJ/mol and 1700 °C with elemental additions of 0, 500, 1000 and 2000 ppm was established using high-resolution synchrotron X-ray powder diffraction and scanning electron microscopy. Microstructural analysis indicates moderate growth of the UO_2 grain structure is achieved with V doping, but not as appreciable as gold-standard Cr-doped UO_2. Collected diffractograms, analysed using the Rietveld method, indicate similar levels of solubility of V in comparison to Cr-doped UO_2 under like conditions. The results of this investigation were discussed in relation to current structural models of lattice incorporation of transition metals in UO_2.

Introduction

The structural-chemical behaviour of UO_2 as transition metal elements are introduced into its structure is of current interest due to the relevance to advanced technology nuclear fuel (ATF) [1] development and fuel-cladding interactions that occur within spent nuclear fuel (SNF) [2]. In the case of ATFs, it has been demonstrated that transition metal elements, such as Cr and Mn, when introduced during fuel fabrication can lead to enhanced grain growth compared to non-doping [3–6]. This leads to enhanced fission gas retention (FGR) during fuel operations, allowing longer burnup cycles and a subsequent reduction of SNF generation per capita compared to regular UO_2-based fuel [7]. At the same time, fuel-cladding interactions in SNF can result in diffusion of specific cladding elements and radionuclides that can impact the overall stability of SNF [8]. The subsequent investigation of chemical incorporation and changes to lattice structure of UO_2 when specific elements, particularly those of the d block, are incorporated is of overall relevance to nuclear fuel development and SNF management.

Recent investigations of Cr- and Mn-doped UO_2 have unveiled the chemical intricacy of relatively trace element doping of the UO_2 structure [3, 4]. In particular, the plethora of secondary chemical phases that can arise impact the solubility within the UO_2 lattice matrix and also the ability of grain growth to occur during material sintering. High-resolution synchrotron X-ray powder diffraction methods were recently demonstrated [9] to provide an almost authoritarian-based tool to probe the changes to the lattice structure and provide insight into the redox changes that occur in UO_2 with transition metal doping. The use of high-resolution methods such as via synchrotron sources to track subtle changes induced from trace doping was crucially highlighted. Consequently, the use of such high-resolution methods to understand changes to structure and material properties is critical to correctly determine the behaviour and performance of novel nuclear materials, particularly those with potential fuel applications.

Vanadium has been a long-term friend of nuclear fuel design and operations, due its low thermal neutron absorption cross section of ^{51}V and its good alloying properties

✉ Gabriel L. Murphy
g.murphy@fz-juelich.de

1 Institute of Fusion Energy & Nuclear Waste Management (IFN-2), Forschungszentrum Jülich GmbH, 52428 Jülich, Germany

2 Institute of Chemistry and Biochemistry, Freie Universität Berlin, 14195 Berlin, Germany

3 Institute of Resource Ecology, Helmholtz-Zentrum Dresden-Rossendorf, 01328 Dresden, Germany

4 The Rossendorf Beamline at ESRF, The European Synchrotron, CS40220, 38043 Grenoble Cedex 9, France

desirable for cladding [7]. Indeed, it has been previously argued that V can induce enhanced grain growth in UO_2, [10, 11] particularly making it applicable for ATF usage. However, there is scarce available literature data on the structural dependence of the UO_2 lattice and microstructure when subject to doping with this element. In light of this, this investigation has utilised high-resolution synchrotron X-ray powder diffraction to examine the structural dependence of the UO_2 lattice structure during additions of 0, 500, 1000 and 2000 ppm V as elemental under conditions of -420 kJ/mol and 1700 °C. Additional to this, the microstructural dependence of the ceramic materials is examined as a function of V addition via scanning electron microscopy.

Experimental

Synthesis of V-doped UO_2 ceramics

V-doped UO_2 ceramics with 0, 500, 1000 and 2000 ppm additions of V element were fabricated using a previously established co-precipitation method beginning with doped ammonium diuranate (ADU) [5]. The doped ADU compounds were prepared using stoichiometrically controlled amounts of uranyl nitrate ($UO_2(NO_3)_2$) and vanadium oxide sulphate ($VOSO_4{\cdot}5H_2O$) that were mixed in solution. To these solutions, ammonia (NH_3) was added at 300% excess, triggering precipitation. The ADU mixtures were calcined under air to oxide form using a box furnace at 800 °C for 5 h prior to reduction to UO_2 at 600 °C under 4% H_2—96% Ar atmosphere for additional 5 h. In both steps, the samples were in powder form. Finally, the pre-treated powders were compacted into pellets and heated to 1700 °C using a tube furnace for 10 h with an oxygen potential (μ_{O2}) of − 420 kJ/mol that was monitored and produced via a 4% H_2—96% Ar and 1% O_2—99% Ar gas mixture. The furnace was cooled to room temperature using a ramp rate of 6 °C/min, whilst the gas mixture was maintained.

Synchrotron X-ray powder diffraction

Ambient temperature synchrotron X-ray powder diffraction (S-XRD) measurements were performed at the BM20 Rossendorf beamline [12] (ROBL) at the European Synchrotron Radiation Facility (ESRF), Grenoble, France. Diffraction data were collected on high-resolution XRD1 machine equipped with a Dectris Eiger CdTe 500 k photon counting detector. Synthesised ceramic samples were finely ground following sintering and immediately packed into glass capillaries of 0.3-mm diameter enclosed in 1-mm Kapton tubes which serve as radiological confinement barriers. The energy of synchrotron radiation was set at 16 000 eV and detector geometry of the experimental setup was calibrated using silver behenate and a LaB_6 NIST standard reference. A precise wavelength of 0.7372 Å was determined. Experiments were performed in a transmission mode Debye–Scherrer geometry and corresponding 2D data were reduced using the PyFAI library adapted for diffractometers mounted on a goniometer arm [13]. Structural analysis was performed using the Rietveld method as implemented in the programme GSAS-II [14]. The peak shapes were modelled using a pseudo-Voigt function and the background was estimated using a 6–12 term shifted Chebyshev function. The scale factor, detector zero-point and lattice parameters were refined together with the peak profile parameters.

Scanning electron microscopy

The morphology of the microstructure of V-doped UO_2 ceramics for 0, 500, 1000 and 2000 ppm elemental additions element was determined using a FEI Quanta 200F (Thermo Fisher Scientific) Scanning Electron Microscope (SEM). Surfaces of parts of the sintered pellets were embedded in resin and carefully polished using diamond pastes (up to 1 µm) and finished with a colloidal Si-suspension. The samples were sputtered with a thin layer of carbon to enhance the electrical conductivity. Back-scattered electron (BSE) images were collected at 10 kV to obtain a high orientation contrast image to identify single grains.

Results and discussion

Collected S-XRD diffractograms were analysed using the Rietveld method where fluorite structural models using the space group $Fm\bar{3}m$ were applied. Rietveld profiles of all analysed diffractograms are provided in Fig. 1, where it can be observed that all generated V-doped UO_2 compounds under described conditions resulted in single phase materials to the limits of resolution. Subtle shifting of Bragg reflections to higher 2θ can be observed in the diffractograms with increasing dopant concentration. This lattice contraction to higher 2θ is consistent with incorporation of the small V cation within the UO_2 lattice matrix, consistent with previous works on Cr- and Mn-doped UO_2 [3, 4, 9]. The lattice parameters determined from Rietveld refinements are provided in Table 1.

SEM micrographs performed on the V-doped UO_2 ceramic pellets fabricated with additions of 0, 500, 1000 and 2000 ppm are provided in Fig. 2. It is evident the addition of V under sintering conditions of − 420 kJ/mol and 1700 °C results in enhanced grain growth compared to the non-doped case. However, this also results in considerable void formation, evident in Fig. 2. The origin of these voids is linked in part to the volatilisation of V which is known to occur under such sintering conditions [15]. In comparison

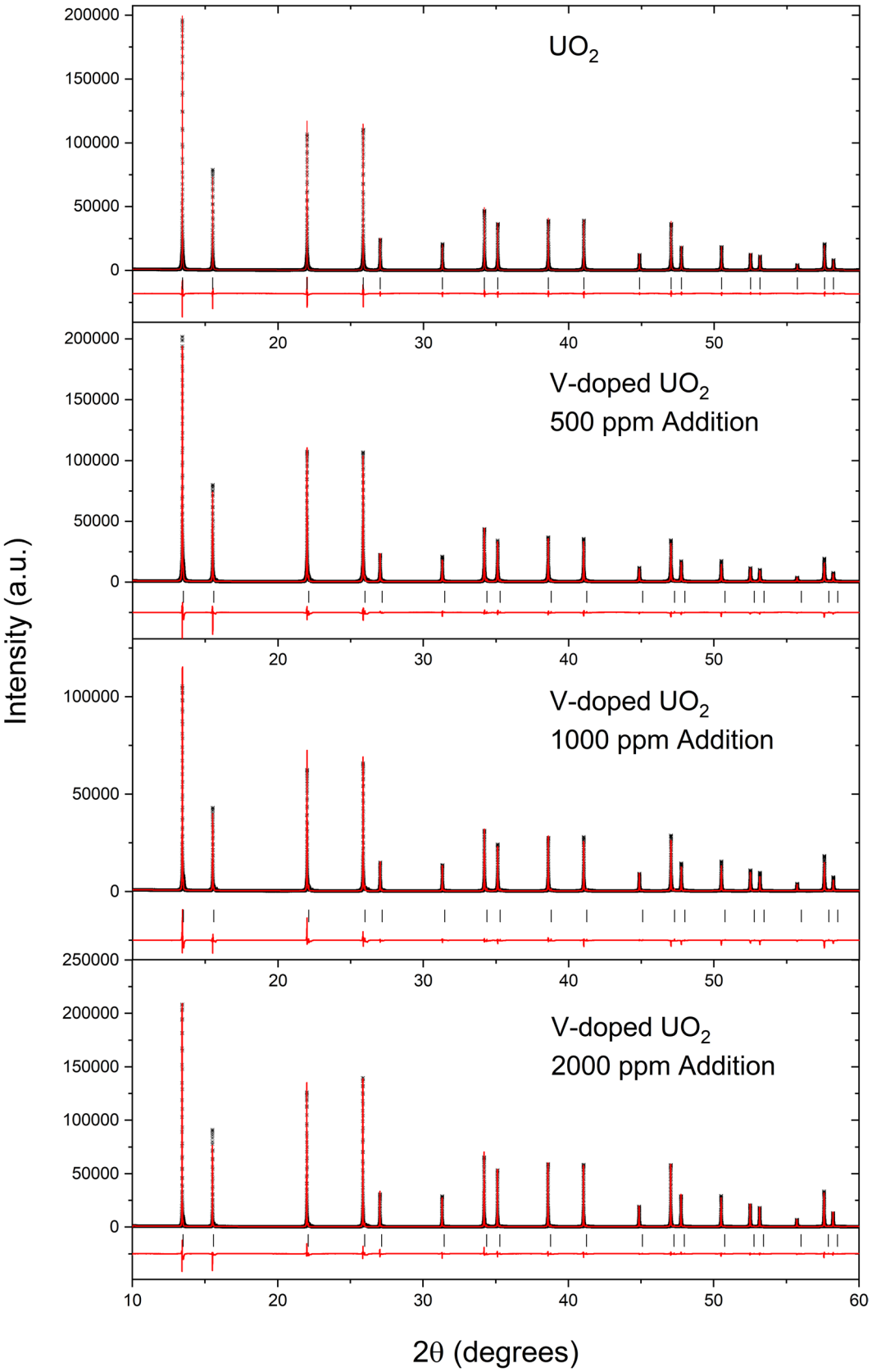

Fig. 1 Rietveld profiles made against S-XRD data collected on V-doped UO_2 powder samples with 0, 500, 1000 and 2000 ppm additions as V elemental for $\lambda = 0.7372$ Å where all structures were refined using a fluorite model in space group $Fm\bar{3}m$

Table 1 Refined lattice parameters for V-doped UO_2 with 0, 500, 1000 and 2000 ppm addition determined from S-XRD data with $\lambda = 0.7372$ Å. The structures were refined in a cubic fluorite structure with space group $Fm\bar{3}m$

V addition ppm	Lattice parameter (Å)	wR_{min} (%)	R_p (%)
0	5.466081 (3)	3.10	10.12
500	5.465646 (5)	2.90	11.59
1000	5.465386 (6)	3.53	11.26
2000	5.465332 (3)	3.02	9.64

to Cr-doped UO_2, under similar doping conditions used for V in the present study, an approximate 100-fold increase in average grain size can be achieved [4]. For V doping of UO_2, there is only a marginal increase in the average grain size compared to undoped UO_2, inferior to what can be achieved with Cr doping [4, 5]. It was recently argued for Mn-UO_2 that the presence of specific secondary phases that arise during UO_2 doping can impact the grain growth process of UO_2 when additives are used, specifically those of fluorite structure which are stable in solid form at sintering conditions [3]. Inspection of the V–O Ellingham diagrams suggests fluorite-based oxides may exist under relevant sintering conditions which can impact grain growth via aforementioned described mechanisms or unwanted volatility that can contribute to porosity [16]. However, this study did not determine whether these phases are present and whether they have a direct impact. Moreover, in the context of additive doped advanced nuclear fuels, these results suggest the doping of UO_2 with V is not as effective as using Cr for enhanced grain growth.

It was recently demonstrated [4, 9] that the normalised changes to the lattice parameter can be used to indirectly track the solubility of dopants within UO_2 and also their redox-structural chemistry. In Fig. 3, the normalised lattice parameters of V-doped UO_2 determined in this study are plotted with reference data from Cr-doped UO_2 and Mn-doped UO_2, [3, 9] synthesised under like conditions and also measured using high-resolution S-XRD.

Inspecting Fig. 3, it is observed that the rate of lattice contraction for V-doped UO_2 with progressive doping is more accelerated than that observed for Cr- and Mn-doped UO_2. For Cr, it is established that there is a solubility limit of 750 ppm for conditions of − 420 kJ/mol and 1700 °C [6]. However, because of the speciation of Cr to different phases other than the UO_2 lattice matrix (Cr_2O_3, Cr-metallic, Cr^{2+} etc.) [4], additions higher than this amount need be performed during synthesis to ultimately reach this solubility limit [9]. This is the reason continuous contraction of the lattice parameter is observed for Cr and Mn above 750 ppm addition [3, 9]. In contrast, for V-doped

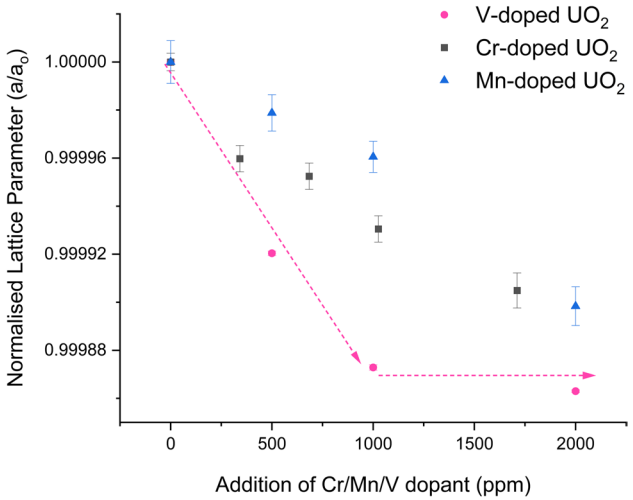

Fig. 3 Normalised lattice parameter (a/a_o) of V-doped UO_2 determined from Rietveld refinements against S-XRD data performed in this work plotted comparatively against lattice parameter data of Mn-doped UO_2 [3] and Cr-doped UO_2 [9] also determined from S-XRD data in which the materials were generated under like conditions of − 420 kJ/mol and 1700 °C. The pink arrows are used as guides to highlight the two different regimes of lattice contraction, prior- and post-solubility limit

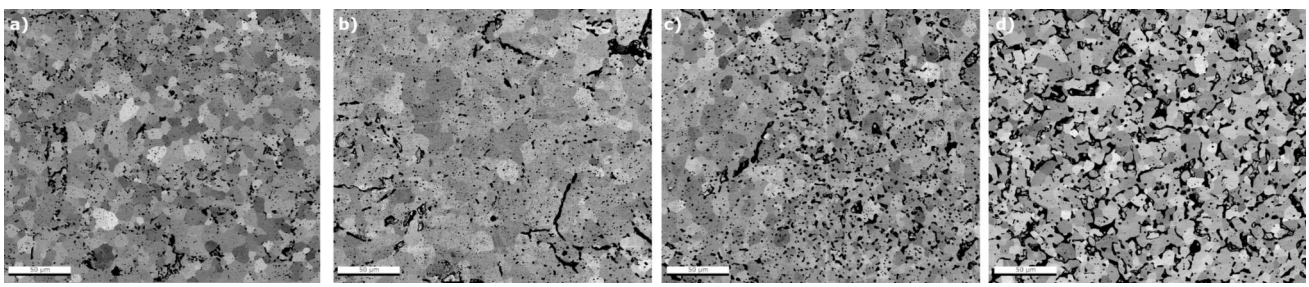

Fig. 2 SEM-BSE images of UO_2 with **a** 0 ppm, **b** 500 ppm, **c** 1000 ppm and **d** 2000 ppm addition of V. Note the subtle increase in average grain size of the microstructure with doping of V which also coincides with an increase in void formation. The void formation is suspected of arising from volatile V oxide species that are lost during sintering, particularly those above the apparent solubility limit of V in UO_2 as identified by S-XRD measurement and analysis

UO_2, linear lattice contraction can be observed between 0 and 1000 ppm V addition which then dramatically changes at 1000 ppm. Between 1000 and 2000 ppm, the change in lattice parameter is relatively negligible, whereas prior to this region constant contraction is observed. Accordingly, this suggests that solubility limit of V within UO_2 has been reached by approximately 1000 ppm addition of V from S-XRD measurement and the solubility is considerably lower than for Cr and Mn. This may explain the enhanced voids observed in SEM micrograph of 2000 ppm compared to the 1000 ppm doping, in which the excess V not contained within the UO_2 matrix, as secondary phases are subject to volatilisation and subsequent contribution to void formation in the microstructure.

Conclusions

A series of V-doped UO_2 ceramic materials with V additions of 0, 500, 1000 and 2000 ppm were synthesised under sintering conditions of − 420 kJ/mol and 1700 °C. The dependence of lattice contraction from V incorporation into the UO_2 lattice was established using S-XRD, in which the data suggest the solubility limit of V within UO_2 is far more diminished than compared to Mn-doped UO_2 and also Cr-doped UO_2. SEM investigation of the microstructure of V-doped UO_2 ceramic pellet specimens indicates that V can induce enhanced grain growth of the UO_2 grain structure, but this is not to the same degree as Cr-doped UO_2, used presently as an ATF for nuclear power generation.

Author contributions The project was conceived and developed by Gabriel L. Murphy. The research methodology, experimental planning and formal analysis were conducted by Gabriel L. Murphy. The materials were synthesized by Gabriel L. Murphy, Julien Marquardt, Philip Kegler, Andrey Bukaemskiy and Maximilian Henkes. Electron microscopy measurements were performed by Martina Klinkenberg. Synchrotron powder diffraction measurements and analysis were performed by Gabriel L. Murphy, Julien Marquardt, Daniil Shirokiy, Dirk Bosbach, Luiza Braga, Selina Richter and Christoph Henig. Manuscript writing, review and editing were performed by Gabriel L. Murphy with input from all authors.

Funding Open Access funding enabled and organized by Projekt DEAL. The authors are grateful to funding and support from the German Federal Ministry of Education and Research (BMBF), Project No. 02NUK060 that enabled this research.

Data availability The data that support the findings of this study are available from the corresponding author, upon reasonable request.

Declarations

Conflict of interest The authors confirm they have no conflicts of interest relating to the contents of this publication.

References

1. I. Greenquist, M. Tonks, M. Cooper, D. Andersson, Y. Zhang, Grand potential sintering simulations of doped UO_2 accident-tolerant fuel concepts. J. Nucl. Mater. **532**, 152052 (2020)
2. R.A. Clark, M.A. Conroy, T.G. Lach, E.C. Buck, K.L. Pellegrini, B.K. McNamara, J.M. Schwantes, Distribution of metallic fission-product particles in the cladding liner of spent nuclear fuel. npj Mater. Degrad. **4**(1), 4 (2020). https://doi.org/10.1038/s41529-019-0107-0
3. G.L. Murphy, E. Bazarkina, A. Rossberg, C.L. Silva, L. Amidani, A. Bukaemskiy, R. Thümmler, M. Klinkenberg, M. Henkes, J. Marquardt et al., The role of redox and structure on grain growth in Mn-doped UO_2. Commun. Mater. **5**(1), 274 (2024). https://doi.org/10.1038/s43246-024-00714-x
4. G.L. Murphy, R. Gericke, S. Gilson, E.F. Bazarkina, A. Rossberg, P. Kaden, R. Thümmler, M. Klinkenberg, M. Henkes, P. Kegler et al., Deconvoluting Cr states in Cr-doped UO_2 nuclear fuels via bulk and single crystal spectroscopic studies. Nat. Commun. **14**(1), 2455 (2023). https://doi.org/10.1038/s41467-023-38109-0
5. P. Kegler, M. Klinkenberg, A. Bukaemskiy, G.L. Murphy, G. Deissmann, F. Brandt, D. Bosbach, Chromium doped UO_2-based ceramics: synthesis and characterization of model materials for modern nuclear fuels. Materials **14**(20), 6160–6178 (2021)
6. C. Riglet-Martial, P. Martin, D. Testemale, C. Sabathier-Devals, G. Carlot, P. Matheron, X. Iltis, U. Pasquet, C. Valot, C. Delafoy, Thermodynamics of chromium in UO_2 fuel: a solubility model. J. Nucl. Mater. **447**(1–3), 63–72 (2014)
7. J.P. Gorton, A.G. Le Coq, Z.G. Wallen, C.M. Petrie, J.T. White, J.T. Dunwoody, S. Mann, N.A. Capps, A.T. Nelson, Modeling and design of a separate effects irradiation test targeting fission gas release from Cr-doped UO_2. Nucl. Eng. Des. **429**, 113571 (2024). https://doi.org/10.1016/j.nucengdes.2024.113571
8. J. Bruno, R.C. Ewing, Spent nuclear fuel. Elements **2**(6), 343–349 (2006)
9. G.L. Murphy, V. Svitlyk, M. Henkes, D. Shirokiy, C. Hennig, P. Kegler, D. Bosbach, A. Bukaemskiy, The lattice contraction of UO2 from Cr doping as determined via high resolution synchrotron X-ray powder diffraction. J. Nucl. Mater. **595**, 155046 (2024). https://doi.org/10.1016/j.jnucmat.2024.155046
10. M.W.D. Cooper, C.R. Stanek, D.A. Andersson, The role of dopant charge state on defect chemistry and grain growth of doped UO_2. Acta Mater. **150**, 403–413 (2018)
11. R.M. Leckie, E.P. Luther, Evolutionary enhancements to UO_2; Los Alamos National Laboratory (LANL), Los Alamos, NM (USA) (2013)
12. A.C. Scheinost, J. Claussner, J. Exner, M. Feig, S. Findeisen, C. Hennig, K.O. Kvashnina, D. Naudet, D. Prieur, A. Rossberg et al., ROBL-II At Esrf: a synchrotron toolbox for actinide research. J. Synchrotron Radiat. **28**(1), 333–349 (2021)

13. J. Kieffer, V. Valls, N. Blanc, C. Hennig, New tools for calibrating diffraction setups. J. Synchrotron Radiat. **27**(2), 558–566 (2020)
14. B.H. Toby, R.B. Von Dreele, GSAS-II: the genesis of a modern open-source all purpose crystallography software package. J. Appl. Crystallogr. **46**(2), 544–549 (2013). https://doi.org/10.1107/S0021889813003531
15. W.X. Wang, Z.L. Xue, S.Q. Song, P. Li, Z.C. Chen, R.N. Liu, G.L. Wang, Research on high-temperature volatilization characteristics of V_2O_5 during direct alloying of smelting vanadium steel. Adv. Mater. Res. **557**, 182–186 (2012)
16. L. Backman, E.J. Opila, Thermodynamic assessment of the group IV, V and VI oxides for the design of oxidation resistant multi-principal component materials. J. Eur. Ceram. Soc. **39**(5), 1796–1802 (2019). https://doi.org/10.1016/j.jeurceramsoc.2018.11.004